Characteristics of Atmospheric Wave–Induced Laminae Observed by Ozonesondes at the Southern Tip of South America

H. Ohyama[1]*, A. Mizuno[1], F. Zamorano[2], T. Sugita[3], H. Akiyoshi[3], K. Noguchi[4], E. Wolfram[5], J. Salvador[5,6,7], and G. C. Benitez[8]

[1]Institute for Space-Earth Environmental Research, Nagoya University, Nagoya, Japan.

[2]University of Magallanes, Punta Arenas, Chile.

[3]National Institute for Environmental Studies, Tsukuba, Japan.

[4]Faculty of Science, Nara Women's University, Nara, Japan.

[5]Laser and Applications Research Center, CEILAP-UNIDEF (MINDEF-CONICET), Villa Martelli, Argentina.

[6]Universidad Tecnológica Nacional, Facultad Regional Buenos Aires (UTN-FRBA) Medrano 951, Buenos Aires, Argentina.

[7]Universidad Nacional de la Patagonia Austral, Unidad Académica Río Gallegos, and CIT Santa Cruz, Río Gallegos, Argentina.

[8]National Meteorological Service, Buenos Aires, Argentina.

*Present address: National Institute for Environmental Studies, Tsukuba, Japan.

Corresponding author: Hirofumi Ohyama (oyama.hirofumi@nies.go.jp)

Key Points:

- Ozonesonde data obtained at southern Patagonia were used to quantify the contribution of gravity waves and Rossby waves to ozone laminae.

- Rossby waves played a dominant role in creating ozone laminae, but the role of gravity waves was not negligible.

- Rossby wave–induced ozone variability was greater inside the polar vortex than outside or near the edge.

Abstract

Fluctuations of ozone concentrations with dimensions of a few kilometers (i.e., ozone laminae) are frequently found in ozone-sounding profiles. We used ozonesonde measurements made at the southern tip of South America to examine the relationship between ozone laminae and atmospheric waves near the edge of the polar vortex and on the leeward side of the Andes Mountains. Laminar structures are formed by vertical and horizontal displacements of isopleths due to gravity waves and by isentropic advection of vortex air filaments with low ozone concentration due to Rossby wave breaking. We extracted components of these ozone fluctuations by applying a high-pass filter to the observed ozone profiles and normalizing them to background concentrations, which were extracted with a low-pass filter. Ozone fluctuations due to displacements caused by gravity waves were individually evaluated with experimental data. We assumed that the residuals between the observed and gravity wave–induced fluctuations were Rossby waves–induced fluctuations. We found that the gravity wave–induced variability was larger in the upper troposphere than in the lower stratosphere and was a maximum in winter. Rossby wave–induced variability showed a distinct seasonal pattern in the lower stratosphere and accounted for a large portion of the observed variability. We also examined the relationship between gravity wave–induced and Rossby wave–induced ozone variability and the differences in equivalent latitudes between the sonde positions and the polar vortex edge. We found that variability was larger inside than outside the polar vortex.

1. Introduction

Ozone concentrations and temperature profiles recorded by sounding balloons have revealed frequent small-scale fluctuations with vertical dimensions of a few kilometers. Because of the relatively long chemical lifetime of ozone, small-scale fluctuations of the ozone volume-mixing ratio below altitudes of ~30 km are functions of mainly atmospheric dynamics such as gravity waves and Rossby waves rather than photochemical processes. Specifically, laminar structures are formed by vertical displacements of isopleths due to gravity waves (Fritts & Alexander, 2003) and by isentropic advection of air mass filaments due to breaking of Rossby waves (Schoeberl & Newman, 1995).

Teitelbaum et al. (1994; 1996) used the relationship between ozone and potential temperature to examine the role of atmospheric waves in producing ozone laminae. Pierce and Grant (1998) and Thompson et al. (2007) used ozonesonde data from the northern hemisphere (NH) mid-latitudes to investigate the correlation between small-scale fluctuations of ozone concentrations and potential temperatures; their goal was to distinguish between the effects of gravity waves and Rossby waves on these fluctuations. Grant et al. (1998) and Thompson et al. (2011) applied the same method to ozonesonde data from tropical and subtropical stations. In the NH mid-latitudes, horizontal motions associated with the breaking of Rossby waves are more prevalent than vertical motions due to gravity waves. In the tropics and subtropics, the dominant vertical motions are associated with gravity waves excited by convection. Noguchi et al. (2006) have used global ozonesonde data from the World Ozone and Ultraviolet Radiation Data Centre to examine the latitudinal variations of small-scale ozone fluctuations. Their analysis has revealed that the ozone fluctuations induced by gravity waves and Rossby waves have an obvious dependence on latitude.

Polar vortex is one of the candidates that cause small-scale ozone fluctuations through Rossby wave breakings. The polar vortex, within which ozone-poor air is isolated from outside air, becomes unstable and breaks up in late spring. Ozone-rich air then intrudes into

the polar region from mid-latitudes and is mixed with the ozone-poor air in the polar region, primarily by adiabatic processes in the horizontal direction. Even before the polar vortex breaks up, weak mixing occurs at the edges of the polar vortex via isentropic equatorward (i.e., outward) or poleward (i.e., inward) advections associated with breaking Rossby waves (e.g., Moustaoui et al., 2003; Nakamura & Plumb, 1994; Waugh et al., 1997). Ozone-rich laminae observed inside the Antarctic ozone hole have been attributed to poleward intrusion of vortex-edge air (Moustaoui et al., 2003; Tomikawa & Sato, 2010). Although the effects of outflows of ozone-poor air on total ozone amounts and ultraviolet indices in the southern hemisphere (SH) mid-latitudes have been investigated (de Laat et al., 2010; Rousseaux et al., 1999; Wolfram et al., 2016), because of the lack of vertical high-resolution data, laminae and variability of ozone concentrations related to the advection and mixing of air masses around the vortex edge have not been thoroughly examined.

Measurements of vertical ozone profiles in the SH mid-latitudes are sparse, in contrast to Antarctica and the SH low-latitudes as well as the NH (e.g., McPeters et al., 2007; Noguchi et al., 2006). Operational ozonesonde measurements in the SH mid-latitudes have been made only at Lauder in New Zealand and Macquarie Island since the 1980s and 1990s, respectively. In 2008, the National Meteorological Service of Argentina initiated operational ozonesonde measurements at Ushuaia (54.85°S, 68.31°W) in Argentina, which is located at the southern tip of South America. In addition, we have performed ozonesonde measurements at Punta Arenas (53.14°S, 70.88°W) in Chile and at Río Gallegos (51.61°S, 69.29°W) in Argentina since 2014 to investigate vertical structures near the edge of the polar vortex as well as to validate ozone profiles measured by a differential absorption lidar and a millimeter-wave radiometer located at Río Gallegos (Orte et al., 2016). Remarkable gravity waves are generated on the leeward side of the Andes in the southern Patagonia area (Sato et al., 2012). The polar vortex contributes both to the generation of the gravity waves by a spontaneous adjustment mechanism and to the formation of the large meridional ozone gradient. Furthermore, the dynamical processes that cause ozone laminae may change as greenhouse gas concentrations increase or ozone depleting substances decrease in the future. For example, the effect of ozone poor air from the spring polar vortex will be reduced when the ozone hole becomes smaller. The effect of gravity waves may change under global warming. The ozone laminae may then change. Thus, since the ozone laminae are closely associated with the dynamics of the troposphere and lower stratosphere, it is important to understand the mechanisms that cause the ozone laminae observed over Patagonia. For this purpose, it is useful to distinguish between the fluctuations in ozone concentration attributed to gravity waves and Rossby waves in the present atmosphere.

The key objectives of this study were to characterize the temporal variations of small-scale ozone fluctuations in the troposphere and stratosphere over Patagonia, where there have been no ozonesonde data available until recently. Specifically, we identified ozone fluctuations that resulted mainly from gravity waves or from Rossby waves within the altitude range of 5–30 km. Gravity waves have a wide range of vertical and horizontal wavelengths, periods, and propagation directions that are location dependent. We examined the temporal variations of the gravity wave characteristics. In addition, during the polar vortex, we evaluated the ozone fluctuations induced by gravity waves and Rossby waves with respect to the differences between the equivalent latitudes of the sonde positions and the edges of the polar vortex.

2. Data

We used ozonesonde data obtained during the period 2008–2016 from Ushuaia (54.85°S, 68.31°W) and Río Gallegos (51.61°S, 69.29°W) in Argentina and from Punta Arenas (53.14°S, 70.88°W) in Chile, all of which are located in southern Patagonia. Tropospheric and stratospheric dynamics over Patagonia are affected by mountain waves (orographic gravity waves) generated on the leeward side of the Andes, non-orographic gravity waves from storms occurring at latitudes of 40–60°S (Trenberth, 1991), and the passage of the polar vortex from the austral winter to spring. The Ushuaia data were taken from the World Ozone and Ultraviolet Radiation Data Centre (https://woudc.org/home.php). Vertical ozone measurements at Ushuaia have been carried out by using electrochemical concentration cell (ECC) ozonesondes and radiosondes (Vaisala, RS92) since April 2008. The ozonesonde data were acquired every month until December 2011, and since 2012 they have been acquired during the winter-to-spring time interval only. Vertical ozone measurements at Río Gallegos and Punta Arenas have been performed with ECC ozonesondes and radiosondes (Lockheed Martin, LMS6) since August 2014. There were only six soundings from Río Gallegos in October 2014. A total of 252 profiles were acquired from the three stations between 2008 and 2016. Ten anomalous profiles, which were identified on the basis of Fourier analysis for each ozone profile, were screened out for purposes of the present study. Figures 1(a) and 1(b) show the numbers of soundings carried out at each station per month and the monthly sounding numbers for each year. Since the amount of ozonesonde data in summer (January and February) is much smaller than that in spring, the features of atmospheric waves and ozone, especially in summer, might not be robust. Therefore, the seasonal variation in wave characteristics and ozone fluctuations will be discussed by comparison with those from other stations located in the SH mid-latitudes and in Antarctica. Figure 1(c) is a histogram of the maximum heights for each sounding. Ozonesondes that reached an altitude of 30 km accounted for approximately 80% of the sounding data for the whole study period.

Figures 2(a) and 2(b) show ozone mixing ratios and temperature profiles recorded by ozonesonde measurements at Ushuaia station on 26 September 2009 and 8 June 2011, respectively. Also shown are the ozone mixing ratios and temperature data from the Modern-Era Retrospective Analysis for Research and Applications-2 (MERRA-2) version of the Goddard Earth Observing System-5 atmospheric general circulation model (Molod et al., 2015; Gelaro et al., 2017), which were interpolated temporally and spatially along the flight paths of the sondes. The observed ozone mixing ratios and temperature profiles were highly perturbed by atmospheric waves, as described in section 3, and the associated laminar structures are apparent in Figure 2. The MERRA-2 ozone profiles were slightly overestimated in the stratosphere compared to the ozonesonde data (c.f., Gelaro et al., 2017). In addition, the laminar structures were not reproduced in the MERRA-2 ozone and temperature profiles. This is probably caused by the relatively coarse resolution of MERRA-2 data and the coarse footprint of Microwave Limb Sounder ozone profile data (165 km for along-track and considerably more for cross-track) used in the MERRA-2 assimilation (Wargan et al., 2015).

3. Analytical methods

In the studies discussed in section 1, the impact of gravity waves on the ozone laminae was taken into account only with respect to the vertical displacement of gravity waves. Rossby waves were assumed to account for the residuals between the observed

fluctuations and those induced by gravity waves (Noguchi et al., 2006). In the present study, we used ozonesonde data from Patagonia, where the horizontal gradient of ozone concentrations is especially large around the polar vortex. Under these conditions, the horizontal displacement of gravity waves may affect ozone laminae. We therefore took into consideration the effects of both horizontal and vertical displacement of gravity waves.

The sonde values of the ozone mixing ratio χ, potential temperature θ, zonal wind u, and meridional wind v were interpolated to an altitude grid with intervals of 0.05 km using a cubic spline interpolation. The noise components in the interpolated data were removed by applying a low-pass filter with a cutoff of 0.5 km. The fluctuating components were obtained by applying a high-pass filter with a cutoff of 4 km to the observed profiles and are designated with a prime ($'$). A fourth-order Butterworth filter was used for smoothing. The fluctuating components were normalized to the background components, which were obtained by applying a low-pass filter with a cutoff of 5 km to the observed profiles, and are expressed by using an overbar ($^-$). Thus, an observed ozone fluctuation is expressed as $\chi'/\overline{\chi}$. Gravity wave–induced laminae stem from vertical displacements of isentropic surfaces and tracer isopleths. An ozone fluctuation resulting from a vertical displacement caused by gravity waves can be represented as follows (e.g., Teitelbaum et al., 1994; Tomikawa et al., 2002):

$$\frac{\chi'_V}{\overline{\chi}} = -\eta'_V \frac{\partial \overline{\chi}}{\partial z}\left(\frac{1}{\overline{\chi}}\right),$$

(1)

where η'_V is the vertical displacement and $\partial \overline{\chi}/\partial z$ is the vertical gradient of the background ozone mixing ratio. The potential temperature fluctuation resulting from the vertical displacement can be represented similarly:

$$\frac{\theta'_V}{\overline{\theta}} = -\eta'_V \frac{\partial \overline{\theta}}{\partial z}\left(\frac{1}{\overline{\theta}}\right).$$

(2)

Because the large-scale motions of Rossby waves do not displace isentropic surfaces (Holton, 1987), equations (1) and (2) can be combined to give equation (3) if one assumes that θ'_V equals θ':

$$\frac{\chi'_V}{\overline{\chi}} = \theta'\left(\frac{\partial \overline{\theta}}{\partial z}\right)^{-1} \frac{\partial \overline{\chi}}{\partial z}\left(\frac{1}{\overline{\chi}}\right).$$

(3)

On the right-hand side of equation (3), the potential temperature fluctuation profiles have been scaled by an altitude-dependent coefficient to compensate for differences in the vertical gradients of the background ozone and potential temperature. We defined the ozone fluctuation resulting from horizontal advection/displacement as the difference between the observed ozone fluctuation and the ozone fluctuation resulting from vertical displacement:

$$\frac{\chi'_H}{\overline{\chi}} = \frac{\chi'}{\overline{\chi}} - \frac{\chi'_V}{\overline{\chi}}. \tag{4}$$

The ozone fluctuation resulting from horizontal displacement due to gravity waves can be represented as follows:

$$\frac{\chi'_{GH}}{\overline{\chi}} = -\eta'_{GH} \frac{\partial \overline{\chi}}{\partial s} \left(\frac{1}{\overline{\chi}} \right), \tag{5}$$

where η'_{GH} is the horizontal displacement due to gravity waves and $\partial \overline{\chi} / \partial s$ is the horizontal gradient of the background ozone mixing ratio. The η'_{GH} displacement can be represented using the wind fluctuation parallel to the direction of horizontal phase propagation of the gravity wave $V'_\parallel$ and an intrinsic frequency $\hat{\omega}$:

$$\frac{\chi'_{GH}}{\overline{\chi}} = -\frac{V'_\parallel}{\hat{\omega}} \frac{\partial \overline{\chi}}{\partial s} \left(\frac{1}{\overline{\chi}} \right). \tag{6}$$

Equation (6) can be rewritten as follows:

$$\frac{\chi'_{GH}}{\overline{\chi}} = -\frac{(u'\cos\phi + v'\sin\phi)}{\hat{\omega}} \left(\frac{\partial \overline{\chi}}{\partial x}\cos\phi + \frac{\partial \overline{\chi}}{\partial y}\sin\phi \right) \left(\frac{1}{\overline{\chi}} \right), \tag{7}$$

where u' and v' are the zonal and meridional wind fluctuations, respectively, and ϕ is the azimuth angle for the direction of horizontal phase propagation of the gravity wave. The values of ϕ and $\hat{\omega}$ were determined from a hodograph analysis (Sato, 1994; Tsuda et al., 1994). Each hodograph analysis was performed using wind vectors at altitudes within ±0.5 km of a given altitude grid. The horizontal wind fluctuation $V'_\parallel$ was obtained by projecting the zonal and meridional wind fluctuations in the horizontal propagation direction. The zonal and meridional gradients of the background ozone mixing ratios (i.e., $\partial \overline{\chi} / \partial x$ and $\partial \overline{\chi} / \partial y$) were calculated by applying a 2.5° low-pass filter to the ozone field data from the MERRA-2. The 2.5° filter that corresponds to the largest horizontal wavelength of gravity waves (i.e., a few hundreds of kilometers as described in section 4.1), was chosen to obtain the ozone fluctuations caused by gravity waves, with small-scale (noisy) structures in the MERRA-2 ozone removed. The ozone fluctuations resulting from horizontal advections caused by Rossby waves were defined as the differences between the observed ozone fluctuations and ozone fluctuations resulting from vertical and horizontal displacements due to gravity waves:

$$\frac{\chi'_R}{\overline{\chi}} = \frac{\chi'}{\overline{\chi}} - \left(\frac{\chi'_V}{\overline{\chi}} + \frac{\chi'_{GH}}{\overline{\chi}} \right). \tag{8}$$

Figure 3(a) shows temperature fluctuations obtained by applying the high-pass filter, which are expressed as a function of altitude relative to tropopause height that was obtained from radiosonde temperature data. Since most temperature profiles sharply bend at the tropopause, the temperature fluctuations after applying the high-pass filter tend to be negatively biased around the tropopause. This structure is related to the thermal tropopause layer, whose strength showed no seasonal variation in the mid-latitudes (Randel et al., 2007). Also shown are the fluctuations of ozone in Figure 3(b), and negative biases similar to the temperature fluctuations are apparent around the tropopause. Therefore, in calculating numerical values such as an arithmetic mean and a root-mean-square (RMS) value within a given altitude range, the data within ±1 km of the tropopause height were excluded.

4. Results and Discussion

4.1. Characteristics of gravity waves in the Patagonia area based on observed meteorological parameters

To characterize the magnitude of gravity waves over Patagonia, the potential energy E of a gravity wave was calculated from equation (9):

$$E = \frac{g^2}{2N^2} \left(\frac{T'}{\overline{T}} \right)^2, \tag{9}$$

where g is the acceleration of gravity, N is the Brunt-Väisälä frequency, T' is the fluctuation of the temperature, and $\overline{T}$ is the mean temperature at a particular altitude (Tsuda et al., 2000; Guharay & Sekar, 2011). Figure 4 shows the seasonal variation of the gravity wave potential energy (GWPE), which was obtained by calculating the arithmetic mean within an altitude range of 5 km and by averaging every five days using the ozonesonde data for the whole period. The GWPE indicated the large values during December to March and June to August in the upper troposphere and during December to May in the lower stratosphere. Operational radiosonde observations at the Falkland Islands (Moffat-Griffin et al., 2013) and Rothera station on the Antarctic Peninsula (Moffat-Griffin et al., 2011) revealed that the GWPE averaged over an altitude range of 15 to 22 km showed different seasonal variations between the two stations. The seasonal variation seen over Patagonia was similar to that over the Falkland Islands, which are at the same latitude as our stations, unlike the Rothera station.

Parameters that characterized the gravity waves—the vertical and horizontal wavelengths, intrinsic period, and vertical and horizontal directions of propagation—were calculated as follows. The observed vertical profiles of temperature, zonal wind, and meridional wind fluctuations over an altitude range of ±0.5 km for a given altitude grid were fitted to sinusoidal curves by least squares; the amplitude and phase were adjusted, and the vertical wavelength was fixed. The optimal vertical wavelengths gave the least fitting residual and were selected from vertical wavelengths in the interval of 0.50–5.00 km in increments of 0.05 km (i.e., 91 fittings). The definitive vertical wavelength was equated to the average of the optimal vertical wavelengths for temperature, zonal wind, and meridional

wind fluctuations. The horizontal wavenumber k was derived by using the dispersion relationship for a gravity wave:

$$\frac{\hat{\omega}^2 - f^2}{N^2 - \hat{\omega}^2} = \frac{k^2}{m^2}, \tag{10}$$

where m is the vertical wavenumber, f is the inertial frequency, and N is the Brunt-Väisälä frequency. The intrinsic period $\hat{\tau}$ was calculated by using the intrinsic frequency $\hat{\omega}$, which was derived from the hodograph analysis (section 3). The horizontal and vertical directions of propagation of the gravity waves were also derived in the hodograph analysis. In the SH, clockwise and counterclockwise rotations of the hodograph of the wind vector with altitude indicate the downward and upward propagation, respectively, of gravity waves in terms of vertical group velocity. The direction of wave propagation is along the major axis of the ellipse of the hodograph, but with an ambiguity of 180°. This ambiguity was removed by using the method described by Hu et al. (2002) and Huang et al. (2017) to exploit the polarization relationship between the horizontal wind fluctuation projected on the assumed direction of propagation and temperature fluctuations.

The vertical and seasonal variations of the vertical wavelengths, horizontal wavelengths, and intrinsic periods of gravity waves, which were obtained by calculating their arithmetic means within a 5-km altitude range and by averaging every five days using the ozonesonde data for the whole period, are shown in Figures 5(a), 5(b), and 5(c), respectively. Figure 6 shows the monthly mean percentages of gravity waves propagating upward and downward in the troposphere and stratosphere. The directions of propagation (upward or downward) were determined individually for gravity waves above and below the altitude of the tropopause, by means of accumulating the respective propagation directions for all profiles within one month. Figure 7 shows the seasonal probability densities of the horizontal propagation directions of gravity waves for four altitude ranges. In the stratosphere, the vertical and horizontal wavelengths, along with their intrinsic periods during the winter and spring season, differ from those in other seasons (Figure 5). The percentage of downward-propagating gravity waves was less than 10% during the summer months of January and February, increasing to approximately 50% in the winter and early spring (from June to September), as shown in Figure 6. This suggests that a gravity wave source in the stratosphere exists mainly in the winter and early spring season. The direction of horizontal propagation in the stratosphere was primarily meridional, especially during winter and spring, as shown in Figures 7(a) and 7(b). A gravity wave resolving aqua-planet model simulated that the gravity waves propagate polewards and equatorwards in the horizontal direction from the polar night jet (Sato & Yoshiki, 2008). We believe that the polar vortex is a gravity wave source in the stratosphere that plausibly explains the results obtained from our radiosonde observations. On the other hand, the main sources of the gravity waves in the troposphere in this geographical region are orographic gravity waves and freely propagating (non-orographic) gravity waves from storms (e.g., Alexander et al., 1995). Below the tropopause, the percentages of upward-propagating and downward-propagating gravity waves were comparable, regardless of the season. The horizontal propagation directions were somewhat more isotropic below than above the tropopause. Thus, the difference in the characteristics of gravity waves in the troposphere and the stratosphere were identified. The effects of the different gravity waves on ozone fluctuations are discussed in the next section.

The seasonal characteristics of propagation in the vertical direction agreed with the results inferred from radiosonde data obtained in the Falkland Islands (Moffat-Griffin et al.,

2013), at Rothera station on the Antarctic Peninsula (Moffat-Griffin et al., 2011), and at Syowa station in Antarctica (Yoshiki et al., 2004). The difference in the estimated direction of horizontal propagation between winter and summer was consistent with results from over Macquarie Island, although the direction of propagation over Macquarie Island in winter is strongly oriented to the south (Vincent et al., 1997). The vertical and horizontal wavelengths in December (~1.5–2.2 km and 50–150 km, respectively) were similar to those in the latitude range 34–48°S, which were obtained from ship-launched radiosonde observations from the end of November to December (Yamamori & Sato, 2006).

We describe in section 4.2 to what extent the fluctuations induced by gravity waves contribute to the observed ozone fluctuations.

4.2. Contributions of gravity and Rossby waves to ozone fluctuations in laminae

Figure 8 shows the observed fluctuations of the ozone mixing ratio ($\chi'/\overline{\chi}$) and the components of the fluctuations of the ozone mixing ratio resulting from vertical displacement due to gravity waves ($\chi'_V/\overline{\chi}$), from horizontal displacement due to gravity waves ($\chi'_{GH}/\overline{\chi}$), and from horizontal advection due to Rossby waves ($\chi'_R/\overline{\chi}$). Figures 8(a) and 8(b) were obtained from the data shown in Figures 2(a) and 2(b), respectively. The observed fluctuations of ozone mixing ratios in Figure 8(a) were characterized by perturbation of up to 50% in the lower stratosphere. Rossby wave–induced fluctuations accounted for most of the fluctuations in Figures 8(a) and 8(b). Gravity wave–induced vertical displacements were apparent at altitudes below 10 km, and gravity wave–induced horizontal displacements occurred in both the troposphere and stratosphere with an amplitude much smaller than that resulting from vertical displacement. In Figure 8(b), although gravity wave–induced fluctuations were in phase with observed fluctuations in most cases, there was one instance when a gravity wave–induced fluctuation was in antiphase with the observed fluctuation (i.e., a Rossby wave–induced fluctuation surpassed the observed fluctuation), as is apparent at an altitude of ~7 km.

We derived ozone variability by calculating the RMS of the ozone fluctuation ($\chi'/\overline{\chi}$) within an altitude range of 5 km and then by shifting up by 0.05 km. Here, we focused on seasonal variations of the ozone variability from data collected over nine years, because of data imbalance in a single year, especially in the summer. Interannual variation in winter and spring with abundant data is discussed in section 4.4. Figure 9 shows the vertical and seasonal variations of observed ozone variability. These variations were obtained by averaging the ozonesonde data for the whole period at 5-day intervals. Below an altitude of ~13 km (in the upper troposphere), ozone variability appears to undergo a seasonal cycle, with a maximum during the winter and a minimum during the summer. We observed a distinct maximum of ozone variability above an altitude of ~13 km (in the lower stratosphere) during the spring. We compare our results with those of Noguchi et al. (2006) in Figure S1, which is the same as Figure 10 except that Figure S1 shows the observed ozone fluctuations not divided by the background component (i.e., χ'), and the vertical scale in Figure S1 is potential temperature. The seasonal cycle in the stratosphere was similar to that derived from ozonesonde measurements at Lauder in New Zealand (Noguchi et al., 2006) and differed above and below ~550 K isentropic surface that corresponds to altitudes of ~20–24 km. The magnitude of the ozone variability in the stratosphere was larger over Patagonia than at Lauder. The longitude band including Patagonia is susceptible to the Antarctic polar vortex due to stationary planetary waves (Grytsai et al., 2007). The polar vortex provides the large

horizontal gradient of ozone, which plays a vital role in creating the ozone laminae. The ozone hole thus might have an impact on the large variability over Patagonia.

Figure 10 shows the vertical and seasonal variations of ozone variability resulting from (a) vertical displacement, (b) horizontal displacement due to gravity waves and advection due to Rossby waves, (c) horizontal displacement due to gravity waves, and (d) horizontal advection due to Rossby waves that were averaged over five-day time intervals. The tropopause heights averaged at 5-day intervals are shown in Figure 10(a). Ozone variability due to vertical displacement was greater in the upper troposphere than in the lower stratosphere and showed seasonal patterns, with a maximum during winter in the upper troposphere, patterns similar to that of the observed (i.e., vertical and horizontal) variability. At altitudes of 13–25 km in the stratosphere, large variability was apparent during summer and autumn. These features were also apparent in the GWPE (Figure 4). As shown in Figure 6, upward-propagating gravity waves were dominant in the summer, but their contribution to vertically propagating waves decreased during the winter. This seasonal pattern was related to critical level filtering of gravity waves propagating upward from the troposphere (Moffat-Griffin et al., 2011, 2013). Our results thus show that gravity waves from the troposphere could affect the seasonal variations of gravity wave–induced ozone laminae in the stratosphere. It is apparent from Figures 10(a) and 10(b) that ozone variability due to horizontal advection/displacement was much larger than that caused by vertical displacement and accounted for a majority of the observed variability.

Ozone variability associated with horizontal displacement due to gravity waves (Figure 10(c)) did not exceed 0.02 and was an order of magnitude smaller than that caused by vertical displacement (Figure 10(a)). Although gravity waves are also created by spontaneous adjustment of flow imbalance around the polar vortex during the winter and spring (McIntyre, 2009), the effects of gravity waves related to the polar vortex were not apparent in our analysis of vertical and horizontal displacements. As described in section 4.1, the effects of the polar vortex were not clearly apparent in the GWPE (Figure 4), and therefore gravity waves related to the polar vortex might have had little influence on the formation of ozone laminae. The contributions of gravity wave–induced variability to the observed variability were approximately 40% and 20% in the upper troposphere and lower stratosphere, respectively, but the Rossby wave–induced variability (Figure 10(d)) still accounted for most of the observed variability (Figure 9). Isentropic advection coupled with vertical wind shear followed the breaking of Rossby waves (Orsolini et al., 1995), and the large gradient of the ozone mixing ratio around the edge of the polar vortex accounted for much of the ozone variability. The mixing of air from inside and outside polar vortex air masses (Schoeberl et al., 1992) might also contribute to large variability in the lower stratosphere during the spring. We note that although we attributed all small-scale fluctuations in the vertical ozone profiles to dynamical mechanisms, photochemical ozone losses in the polar vortex may moderately impact the amplitude of ozone fluctuations resulting from Rossby wave breakings.

Figures S2 and S3 in the supporting information illustrate ozone variability similar to that seen in Figures 10(a) and 10(b), respectively; however, Figures S2 and S3 show ozone fluctuations that have not been divided by the background component, and the vertical scales are represented by potential temperature. A comparison to results at other stations shown by Noguchi et al. (2006) revealed that the ozone variability resulting from gravity waves and Rossby waves over Patagonia was largest among several stations located within the same latitude bands in the NH and the SH. This result appears to reflect local effects such as the Andes and the polar vortex, as described above.

In section 3, although it is assumed that fluctuations of potential temperature would be caused exclusively by vertical displacements due to gravity waves, the fluctuations may be caused by other processes, for example, horizontal advection of a filament of air (Richter & Atkinson, 1999). Instead of the potential temperature fluctuations, we used horizontal wind fluctuations, which are only induced by gravity waves, to calculate the ozone fluctuation resulting from the vertical displacement due to gravity waves using equation (11) (Gibson-Wilde et al., 1997):

$$\frac{\chi'_V}{\overline{\chi}} = -\frac{iV'_\parallel}{N}\sqrt{1 - \left(\frac{f}{\hat{\omega}}\right)}\frac{\partial\overline{\chi}}{\partial z}\left(\frac{1}{\overline{\chi}}\right), \tag{11}$$

where i is the imaginary unit. Because the horizontal wind fluctuations have a phase difference of 90° compared with ozone fluctuations, we focused on ozone variability (amplitude) rather than ozone fluctuations. Figure 11(a) shows the seasonal variation of the ozone variability from the vertical displacement calculated from equation (11). Comparing with Figure 10(a), the ozone variability by vertical displacements calculated from the horizontal wind and potential temperature fluctuations showed a similar seasonal variation. The relative difference between Figures 10(a) and 11(a) (i.e., (Figure 10(a) – Figure 11(a)) / Figure 11(a) × 100)) is shown in Figure 11(b). In the stratosphere, the ozone variability calculated from the potential temperature fluctuations (Figure 10(a)) was generally smaller than that calculated from the horizontal wind fluctuations (Figure 11(a)). Although we do not know the cause of the difference, the effects of advection of filamentary air (as described above), which would result in larger ozone variability for the potential temperature fluctuations, were not apparent. Below the tropopause region, the ozone variability in Figure 10(a) was larger than that in Figure 11(a). Around the tropopause, the tropopause inversion layer, which is evident in both the temperature and wind data based on radiosonde measurements (Birner, 2006), may be responsible for the potential temperature and wind fluctuations. In the upper troposphere, disturbances associated with extratropical cyclones may cause the potential temperature and wind fluctuations. It is presumed that the tropopause inversion layer and atmospheric disturbance have a larger impact on the potential temperature fluctuations than on the wind fluctuations. The causes of the differences between Figures 10(a) and 11(a) should be further examined by taking into account results from other stations.

4.3. Occurrence frequency of ozone laminae resulting from gravity and Rossby waves based on the correlation between ozone and potential temperature fluctuations

Another way to determine whether the main causes of the ozone laminae were gravity waves or Rossby waves is to apply a classification scheme based on the correlation coefficients between the normalized ozone fluctuations and the scaled potential temperature fluctuations, an approach suggested by Pierce and Grant (1998). Using the methodology of Pierce and Grant (1998), we classified the ozone variations into five types: low variability; gravity waves; Rossby waves; both gravity waves and Rossby waves; and unknown. We first investigated the magnitude of the ozone variability (i.e., the RMS of the normalized ozone fluctuations) within each altitude interval. Because the precision of the ozonesonde measurements was ~5% (Smit et al., 2007), we assigned data with a RMS <5% to the low variability category. For data with an RMS >5%, we then examined the correlation coefficient (R) between the observed ozone fluctuation ($\chi'/\overline{\chi}$) and the scaled potential

temperature fluctuation (equation (3)) within an altitude range of 5 km. Rossby wave–induced laminae were not correlated with potential temperature fluctuations, whereas gravity wave–induced laminae were correlated. To classify the ozone variations, we adopted thresholds for the correlation coefficient that were arbitrarily determined in the previous study (Pierce & Grant, 1998) and have also been used in related studies (e.g., Thompson et al., 2007). The use of the same threshold as in previous studies enables the comparison of our results with those from other stations. Specifically, if the correlation coefficient exceeded 0.7, we attributed the variation to vertical displacement. Similarly, we attributed the variation to both gravity waves and Rossby waves if the correlation coefficient was 0.3–0.7, and to Rossby waves alone if the correlation coefficient was in the range −0.3 to 0.3. Finally, if the correlation coefficient was less than −0.3, we considered the cause of the variation to be unknown.

The vertical and seasonal variations of the correlation coefficients between ozone and scaled potential temperature fluctuations were averaged every five days using the ozonesonde data for the whole period (Figure 12). In the upper troposphere, the correlation coefficients were relatively high throughout the year. The high correlations were likely due to the fact that the ozone fluctuations in this altitude range resulted from vertical displacements of isopleths due to gravity waves. The correlation coefficients in the lower stratosphere (altitudes of 13–20 km) during winter and spring were close to zero. We attributed this lack of correlation to frequent generation of laminae by quasi-isentropic advections associated with Rossby waves. Although the correlation coefficients for the lower stratosphere in autumn were large, the variability due to gravity waves was small, as is apparent in Figure 10(a). The reason for these high correlation coefficients is unclear; one possibility is that the ozone fluctuations due to Rossby waves were coincidentally in phase with the fluctuations due to gravity waves.

Table 1 lists the occurrence frequency of each type of ozone variation on the basis of the correlation coefficients between ozone and scaled potential temperature fluctuations for four altitude ranges: 5 km to the tropopause; the tropopause to 15 km; 15–20 km; and 20–25 km. Because the variability was low at altitudes of 20–25 km, we discuss the occurrence frequencies for the altitude range of 5–20 km. Below 20 km, more than one-third of the laminae were attributed to both gravity waves and Rossby waves (i.e., $0.3 < R < 0.7$). The occurrence frequencies of laminae induced mainly by gravity waves and by Rossby waves were relatively high below 15 km and between the tropopause and 20 km, respectively. Although it is not possible to directly compare these results with the atmospheric wave–induced ozone variability described in section 4.2, we found that these results for the occurrence frequency exhibited a tendency similar to the vertical distribution of ozone variability resulting from gravity waves or Rossby waves (Figure 10). Thus, although the choice of thresholds for the correlation coefficient is arbitrary, this choice of thresholds seems reasonable when identifying the ozone variation.

In the tropics and subtropics, the occurrence frequencies of gravity wave–induced laminae stand out (more than 40%) above the tropopause because of the frequent occurrence of convective gravity waves, whereas Rossby wave–induced laminae accounted for <20% of ozone variations in both the upper troposphere and lower stratosphere, likely because of the low horizontal gradient of ozone (Thompson et al., 2011). In the NH mid-latitudes (e.g., Wallops Island, 37.5°N, 75.3°E), the occurrence frequencies of gravity wave– and Rossby wave–induced laminae are comparable, with percentages as high as 25% (Pierce & Grant, 1998). The ozone laminae over Patagonia were characterized by gravity wave–induced laminae, the occurrence frequency of which was higher in the upper troposphere than in the lower stratosphere, and by Rossby wave–induced laminae, with occurrence frequencies >30% in the lower stratosphere.

4.4. Relationship between ozone variability and equivalent latitude

In section 4.2, we showed that the seasonal variations of Rossby wave–induced ozone variability reached a maximum in the spring, when the polar vortex was present. In this section, we evaluate whether the ozone variability was associated with the position relative to the polar vortex.

To determine whether the ozonesonde was located outside, near the edge, or inside the polar vortex, we calculated the equivalent latitudes of the edges of the polar vortex and the ozonesonde positions on isentropic surfaces of 375, 450, and 550 K, which roughly correspond to the centers of the following altitude ranges: tropopause to 15 km, 15–20 km, and 20–25 km. The equivalent latitude was defined as the latitude enclosing the same area as a potential vorticity contour. The potential vorticity data were taken from the MERRA-2 reanalysis. The edge position and the edge region of the polar vortex were determined from the first and second derivatives, respectively, of potential vorticity with respect to equivalent latitude, in accord with Nash et al. (1996). The equivalent latitudes for the polar vortex (edge position, inner boundary, and outer boundary) were temporally smoothed by averaging the calculated equivalent latitudes that were within ±24 h of the time of the ozonesonde measurement.

Figure 13 shows the gravity wave–induced and Rossby wave–induced variability between July and November for the three altitude ranges as a function of the differences in the equivalent latitudes between the sonde positions and the polar vortex edges on 375, 450, and 550 K isentropic surfaces. The sonde positions relative to the polar vortex were classified into three categories (i.e., inside, near the edge, and outside the polar vortex) because the width of the edge region varied with the season and year. Because the ozone-mixing ratio varied greatly in the polar vortex edge region, large variability was anticipated around this region (Manney et al., 2005; Mariotti et al., 2000; Pierce et al., 1997). The gravity wave–induced variability did not show a significant dependence on the positions of the sonde and polar vortex for each isentropic surface although the variability at an altitude range of 20–25 km appeared to be slightly larger inside the polar vortex than outside. The magnitude of the gravity wave–induced variability increased with decreasing altitude. At altitudes of 15–20 km and 20–25 km, the Rossby wave–induced variability was larger inside the polar vortex than outside or near the edge. Outside the polar vortex, the laminae may have been rapidly dispersed as a result of horizontal diffusion from the surrounding air to the filament air. Roscoe et al. (2012) observed that the variability of ozone concentrations was larger inside the polar vortex than near the edge on the basis of trajectories of long-duration balloons over Antarctica. According to dynamical analyses (de la Camara et al., 2013; Lee et al., 2001), the edge region of the Antarctic polar vortex remains nearly unaffected by mixing with the air inside the vortex and acts as a barrier to transport of air mass. It is therefore difficult for laminae to form in the edge region. The dynamical isolation of the vortex-edge air thus contributes to the differences in ozone variability between the vortex edge and interior of the vortex.

Rossby wave activity has interannual variation and is known to impact the breakup date of the Antarctic polar vortex (Hurwitz et al., 2010). Figure 14 shows the relationship between the Rossby wave-induced variability between June and November and the day of the final breakdown of the Antarctic polar vortex for each year, defined as the day when the ozone hole area first became zero (https://ozonewatch.gsfc.nasa.gov/meteorology/ozone_2016_MERRA2_SH.html). We must note that the annual variation of the Rossby wave-induced variability was not statistically significant, as apparent from the error bars that are almost equal to the range of the annual

variation. Nevertheless, it can be observed that when the Rossby wave-induced variability was larger, the final breakdown tends to take place earlier in the year. This result implies that the Rossby waves are related to the evolution of the Antarctic polar vortex and the ozone variability derived from ozone laminae could be a measure of dynamical activity.

5. Conclusions

We used ozonesonde data obtained at Ushuaia and Río Gallegos in Argentina and Punta Arenas in Chile to quantify the contribution of gravity waves and Rossby waves to the laminae observed in vertical ozone concentration profiles. Over Patagonia, notable gravity waves are generated on the leeward side of the Andes and around the polar vortex by a spontaneous adjustment mechanism. The polar vortex could also contribute to the formation of large meridional ozone gradients associated with laminae as a result of horizontal advection/displacement. Ozone fluctuations caused by vertical and horizontal displacements due to gravity waves were calculated from ozone, temperature, and wind data collected by sondes and from the MERRA-2 ozone field data. The ozone fluctuations resulting from Rossby waves were assumed to be the residuals between the observed and gravity wave–induced fluctuations. The gravity wave–induced variability in the upper troposphere showed a seasonal pattern with a maximum in winter, whereas that in the lower stratosphere indicated the large values during the summer-to-autumn time interval. The Rossby wave–induced variability had a distinct seasonal variation in the lower stratosphere that reached a maximum in spring. We found that the gravity wave–induced variability accounted for a small part (approximately 40% in the upper troposphere and 20% in the lower stratosphere) of the observed variability. By examining the correlations between ozone and scaled potential temperature fluctuations, the occurrence frequencies of the ozone laminae resulting from gravity waves and Rossby waves were derived within four altitude ranges: 5 km to the tropopause; tropopause to 15 km; 15–20 km; and 20–25 km. The occurrence frequency of laminae induced mainly by gravity waves was less than 20%. We thus found that Rossby waves played a dominant role in creating ozone laminae over Patagonia, but the role of gravity waves was not negligible. In addition, we investigated the gravity wave–induced and Rossby wave–induced ozone variability with respect to the edges of the polar vortex. We found that Rossby wave–induced ozone variability was greater inside the polar vortex than outside or near the edge.

Although we found that Rossby waves accounted for most ozone laminae in the southern part of South America, investigations at higher latitudes and different longitude will be conducted by future studies. When the magnitude of the ozone hole decreases in the future, the large variability of ozone concentrations due to Rossby waves from near the edge to the interior of the polar vortex will become smaller.

References

Alexander, M. J., Holton, J. R., & Durran, D. R. (1995). The gravity-wave response above deep convection in a squall line simulation. J. Atmos. Sci., 52(12), 2212–2226.

Birner, T. (2006). Fine-scale structure of the extratropical tropopause region. J. Geophys. Res., 111, D04104. https://doi.org/10.1029/2005JD006301

de Laat, A. T. J., van der A, R. J., Allaart, M. A. F., van Weele, M., Benitez, G. C., Casiccia, C., et al. (2010). Extreme sunbathing: Three weeks of small total O_3 columns and high UV radiation over the southern tip of South America during the 2009 Antarctic O_3 hole season. Geophys. Res. Lett., 37, L14805. https://doi.org/10.1029/2010GL043699

de la Camara, A., Mechoso, C. R., Mancho, A. M., Serrano, E., & Ide, K. (2013). Isentropic transport within the Antarctic polar-night vortex: Rossby wave breaking evidence and Lagrangian structures. J. Atmos. Sci., 70(9), 2982–3001. https://doi.org/10.1175/JAS-D-12-0274.1

Fritts, D. C., & Alexander, M. J. (2003). Gravity wave dynamics and effects in the middle atmosphere. Rev. Geophys., 41(1), 1003. https://doi.org/10.1029/2001RG000106

Gelaro, R., McCarty, W., Suárez, M. J., Todling, R., Molod, A., Takacs, L., et al. (2017). The Modern-Era Retrospective Analysis for Research and Applications, Version 2 (MERRA-2). J. Clim., 30, 5419–5454. https://doi.org/10.1175/JCLI-D-16-0758.1

Gibson-Wilde, D. E., Vincent, R. A., Souprayen, C., Godin, S., Hertzog A., & Eckerman, S. D. (1997) Dual lidar observations of mesoscale fluctuations of ozone and horizontal winds. Geophys. Res. Lett., 24(13), 1627-1630. https://doi.org/10.1029/97GL01609

Grant, W. B., Pierce, R. B., Oltmans, S. J., & Browell, E. V. (1998). Seasonal evolution of total and gravity wave induced laminae in ozonesonde data in the tropics and subtropics. Geophys. Res. Lett., 25, 1863–1866. https://doi.org/10.1029/98GL01297

Grytsai, A. V., Evtushevsky, O. M., Agapitov, O. V., Klekociuk, A. R., & Milinevsky, G. P. (2007). Structure and long-term change in the zonal asymmetry in Antarctic total ozone during spring. Ann. Geophys., 25(2), 361–374.

Guharay, A., & Sekar, R. (2011). Seasonal characteristics of gravity waves in the middle atmosphere over Gadanki using Rayleigh lidar observations. J. Atmos. Sol. Terr. Phys., 73, 1762–1770. https://doi.org/10.1016/j.jastp.2011.04.013

Holton, J. R. (1987). The production of temporal variability in trace constituent concentrations. In G. Visconti & R. Garcia (Eds.), Transport Process in the Middle Atmosphere, NATO ASI Series, (Vol. 213, pp. 313–326). New York, NY: Springer.

Hu, X., Liu, A. Z., Gardner, C. S., & Swenson, G. R. (2002). Characteristics of quasi-monochromatic gravity waves observed with Na lidar in the mesopause region at Starfire Optical Range, NM. Geophys. Res. Lett., 29(24), 2169. https://doi.org/10.1029/2002GL014975

Huang, K. M., Liu, A. Z., Zhang, S. D., Yi, F., Huang, C. M., Gong, Y., et al. (2017). Simultaneous upward and downward propagating inertia-gravity waves in the MLT observed at Andes Lidar Observatory. J. Geophys. Res. Atmos., 122. https://doi.org/10.1002/2016JD026178

Hurwitz, M. M., Newman, P. A., Li, F., Oman, L. D., Morgenstern, O., Braesicke, P., & Pyle, J. A. (2010). Assessment of the breakup of the Antarctic polar vortex in two new chemistry-climate models. J. Geophys. Res., 115, D07105. http://doi.org/10.1029/2009JD012788

Lee, A. M., Roscoe, H. K., Jones, A. E., Haynes, P. H., Shuckburgh, E. F., Morrey, M. W., & Pumphrey, H. (2001). The impact of the mixing properties within the Antarctic stratospheric vortex on ozone loss in spring. J. Geophys. Res., 106 (D3), 3203–3211. https://doi.org/10.1029/2000JD900398

Manney, G. L., Santee, M. L., Livesey, N. J., Froidevaux, L., Read, W. G., Pumphrey, H. C., et al. (2005). EOS Microwave Limb Sounder observations of the Antarctic polar vortex breakup in 2004. Geophys. Res. Lett., 32, L12811. https://doi.org/10.1029/2005GL022823

Mariotti, A., Mechoso, C. R., Legras, B., & Daniel, V. (2000). The evolution of the ozone "collar" in the Antarctic lower stratosphere during early August 1994. J. Atmos. Sci., 57, 402–414. https://doi.org/10.1175/1520-0469(2000)057<0402:TEOTOC>2.0.CO;2

McIntyre, M. E. (2009). Spontaneous imbalance and hybrid vortex–gravity structures. J. Atmos. Sci., 66, 1315–1326. https://doi.org/10.1175/2008JAS2538.1

McPeters, R. D., Labow, G. J., & Logan, J. A. (2007). Ozone climatological profiles for satellite retrieval algorithms. J. Geophys. Res., 112, D05308. https://doi.org/10.1029/2005JD006823

Moffat-Griffin, T., Hibbins, R. E., Jarvis, M. J., & Colwell, S. R. (2011). Seasonal variations of gravity wave activity in the lower stratosphere over an Antarctic Peninsula station. J. Geophys. Res., 116, D14111. https://doi.org/10.1029/2010JD015349

Moffat-Griffin, T., Jarvis, M. J., Colwell, S. R., Kavanagh, A. J., Manney, G. L., & Daffer, W. H. (2013). Seasonal variations in lower stratospheric gravity wave energy above the Falkland Islands. J. Geophys. Res. Atmos., 118, 10,861–10,869. https://doi.org/10.1002/jgrd.50859

Molod, A., Takacs, L., Suarez, M., & Bacmeister, J. (2015). Development of the GEOS-5 atmospheric general circulation model: evolution from MERRA to MERRA2. Geosci. Model Dev., 8, 1339–1356. https://doi.org/10.5194/gmd-8-1339-2015

Moustaoui, M., Teitelbaum, H., & Valero, F. P. J. (2003). Ozone laminate inside the Antarctic vortex produced by poleward filaments. Q. J. R. Meteorol. Soc., 129, 3121–3136. https://doi.org/10.1256/003590003769682200

Nakamura, M., & Plumb, R. A. (1994). The effects of flow asymmetry on the direction of Rossby wave breaking. J. Atmos. Sci., 51, 2031–2045.

Nash, E. R., Newman, P. A., Rosenfield, J. E., & Schoeberl, M. R. (1996). An objective determination of the polar vortex using Ertel's potential vorticity. J. Geophys. Res., 101, 9471–9478. https://doi.org/10.1029/96JD00066

Noguchi, K., Imamura, T., Oyama, K.-I., & Bodeker, G. E. (2006). A global statistical study on the origin of small-scale ozone vertical structures in the lower stratosphere. J. Geophys. Res., 111, D23105. https://doi.org/10.1029/2006JD007232

Orsolini, Y., Simon, P., & Cariolle, D. (1995). Filamentation and layering of an idealized tracer by observed winds in the lower stratosphere. Geophys. Res. Lett., 22, 839–842. https://doi.org/10.1029/95GL00389

Orte, F., Salvador, J., Wolfram, E., D'Elia, R., Quiroga, J., Zamorano, F., et al. (2016). Stratospheric and Mesospheric Ozone Profile Intercomparison at OAPA, Río Gallegos. Paper presented at Quadrennial Ozone Symposium 2016, Edinburgh, United Kingdom.

Pierce, R. B., & Grant, W. B. (1998). Seasonal evolution of Rossby and gravity wave induced laminae in ozonesonde data obtained from Wallops Island, Virginia. Geophys. Res. Lett., 25, 1859–1862. https://doi.org/10.1029/98GL01507

Pierce, R. B., Grooss, J.-U., Grose, W. L., Russell III, J. M., Crutzen, P. J., Fairlie, T. D., & Lingenfelser, G. (1997). Photochemical calculations along air mass trajectories during ASHOE/MAESA. J. Geophys. Res., 102, 13153–13167. https://doi.org/10.1029/96JD03506

Randel, W. J., Wu, F., & Forster, P. (2007). The extratropical tropopause inversion layer: Global observations with GPS data, and a radiative forcing mechanism. J. Atmos. Sci., 64, 4489–4496. https://doi.org/10.1175/2007JAS2412.1

Richter, H. & Atkinson, R. J. (1999) The signature of cyclonic PV filaments in the lower stratosphere. J. Geophys. Res., 104, D20, 24281-24295. https://doi.org/10.1029/1999JD900829

Roscoe, H. K., Feng, W., Chipperfield, M. P., Trainic, M., & Shuckburgh, E. F. (2012). The existence of the edge region of the Antarctic stratospheric vortex. J. Geophys. Res., 117, D04301. https://doi.org/10.1029/2011JD015940

Rousseaux, M. C., Ballaré, C. L., Giordano, C. V., Scopel, A. L., Zima, A. M., Szwarcberg-Bracchitta, M., et al. (1999). Ozone depletion and UVB radiation: Impact on plant DNA damage in southern South America. Proc. Natl. Acad. Sci., 96, 15310–15315. https://doi.org/10.1073/pnas.96.26.15310

Sato, K. (1994). A statistical study of the structure, saturation and sources of inertio-gravity waves in the lower stratosphere observed with the MU radar. J. Atmos. Terr. Phys., 56, 755–774.

Sato, K., & Yoshiki, M. (2008). Gravity wave generation around the polar vortex in the stratosphere revealed by 3 hourly radiosonde observations at Syowa Station. J. Atmos. Sci., 65(12), 3719–3735. https://doi.org/10.1175/2008JAS2539.1

Sato, K., Tateno, S., Watanabe, S., & Kawatani, Y. (2012). Gravity wave characteristics in the Southern Hemisphere revealed by a high-resolution middle atmosphere general circulation model. J. Atmos. Sci., 69, 1378–1396. https://doi.org/10.1175/JAS-D-11-0101.1

Schoeberl, M. R., & Newman, P. A. (1995). A multiple-level trajectory analysis of vortex filaments. J. Geophys. Res., 100, 25,801–25,815. https://doi.org/10.1029/95JD02414

Schoeberl, M. R., Lait, R., Newman, P. A., & Rosenfield, J. E. (1992). The structure of the polar vortex. J. Geophys. Res., 97, 7859–7882. https://doi.org/10.1029/91JD02168

Smit, H. G. J., Straeter, W., Johnson, B. J., Oltmans, S. J., Davies, J., Tarasick, D. W., et al. (2007). Assessment of the performance of ECC-ozonesondes under quasi-flight conditions in

the environmental simulation chamber: Insights from the Juelich Ozone Sonde Intercomparison Experiment (JOSIE). J. Geophys. Res., 112, D19306. https://doi.org/10.1029/2006jd007308

Teitelbaum, H., Ovarlez, J., Kelder, H., & Lott, F. (1994). Some observations of gravity-wave-induced structure in ozone and water vapour during EASOE. Geophys. Res. Lett., 21(13), 1483–1486. https://doi.org/10.1029/93GL02434

Teitelbaum, H., Moustaoui, M., Ovarlez, J., & Kelder, H. (1996). The role of atmospheric waves in the laminated structure of ozone profiles at high latitudes. Tellus, Ser. A, 48, 442–455.

Thompson, A. M, Stone, J. B., Witte, J. C., Miller, S. K., Pierce, R. B., Chatfield, R. B., et al. (2007). Intercontinental Transport Experiment Ozonesonde Network Study (IONS, 2004): 1. Summertime Upper Troposphere/Lower Stratosphere (UT/LS) Ozone over Northeastern North America. J. Geophys. Res., 112, D12S12. https://doi.org/10.1029/2006JD007441

Thompson, A. M., Allen, A. L., Lee, S., Miller, S. K., & Witte, J. C. (2011). Gravity and Rossby wave signatures in the tropical troposphere and lower stratosphere based on Southern Hemisphere Additional Ozonesondes (SHADOZ), 1998–2007. J. Geophys. Res., 116, D05302. https://doi.org/10.1029/2009JD013429

Tomikawa, Y., & Sato, K. (2010). Ozone enhanced layers in the 2003 Antarctic ozone hole. J. Meteorol. Soc. Jpn., 88, 1–14. https://doi.org/10.2151/jmsj.2010-101

Tomikawa, Y., Sato, K., Kita, K., Fujiwara, M., Yamamori, M., & Sano, T. (2002). Formation of an ozone lamina due to differential advection revealed by intensive observations. J. Geophys. Res., 107(D10), 4092. https://doi.org/10.1029/2001JD000386

Trenberth, K. E. (1991). Storm tracks in the Southern Hemisphere. J. Atmos. Sci., 48, 2159–2178.

Tsuda, T., Murayama, Y., Wiryosumarto, H., Harijono, S., & Kato, S. (1994). Radiosonde observations of equatorial atmosphere dynamics over Indonesia: 2. Characteristics of gravity-waves. J. Geophys. Res., 99(D4), 10,507–10,516. https://doi.org/10.1029/94JD00354

Tsuda, T., Nishida, M., Rocken, C., & Ware, R. H. (2000). A global morphology of gravity wave activity in the stratosphere revealed by the GPS occultation data (GPS/MET). J. Geophys. Res., 105(D6), 7257–7274. https://doi.org/10.1029/1999JD901005

Vincent, R. A., Allen, S. J., & Eckermann, E. (1997). Gravity-wave parameters in the lower stratosphere. In K. Hamilton (Eds.), Gravity Wave Processes: Their Parameterization in Global Climate Models (pp. 7–25). New York, NY: Springer-Verlag.

Wargan, K., Pawson, S., Olsen, M. A., Witte, J. C., Douglass, A. R., Ziemke, J. R., et al. (2015). The global structure of upper troposphere-lower stratosphere ozone in GEOS-5: a multiyear assimilation of EOS Aura data. J. Geophys. Res. Atmos., 120, 2013–2036. http://dx.doi.org/10.1002/2014JD022493

Waugh, D. W., Plumb, R. A., Elkins, J. W., Fahey, D. W., Boering, K. A., Dutton, G. S., et al. (1997). Mixing of polar vortex air into middle latitude as revealed by tracer-tracer scatterplots. J. Geophys. Res., 102, 13119–13134. https://doi.org/10.1029/96JD03715

Wolfram, E. W., Orte, P. F., Salvador, J. O., Pazmiño, A., Godin-Beekmann, S., Quel, E. J., et al. (2016). Transport of low ozone air masses to South America middle latitudes: impact on solar UV irradiances. Paper presented at Quadrennial Ozone Symposium 2016, Edinburgh, United Kingdom.

Yamamori, M., & Sato, K. (2006). Characteristics of inertia gravity waves over the South Pacific as revealed by radiosonde observations. J. Geophys. Res., 111, D16110. https://doi.org/10.1029/2005JD006861

Yoshiki, M., Kizu, N., & Sato, K. (2004). Energy enhancements of gravity waves in the Antarctic lower stratosphere associated with variations in the polar vortex and tropospheric disturbances. J. Geophys. Res., 109, D23104. https://doi.org/10.1029/2004JD004870

Table 1. *Percentages of Ozone Variation Associated with Low Variability, Gravity Waves (GWs), Rossby Wave (RWs), Both GWs and RWs, and Unknown.*

Altitude ranges	Low variability (RMS < 5%)	GW ($R > 0.7$)	GW and RW ($0.3 < R < 0.7$)	RW ($|R| < 0.3$)	Unknown ($R < -0.3$)
5 km–TPH[a]	2	18	43	32	5
TPH–15 km	4	11	35	45	5
15–20 km	11	7	39	38	5
20–25 km	73	8	8	9	2

Note. Assignments were made on the basis of correlation coefficients (R) between ozone and scaled potential temperature fluctuations for each altitude range. The percentages of ozone variation were calculated using sounding data for the whole study period.

[a]TPH, tropopause height.
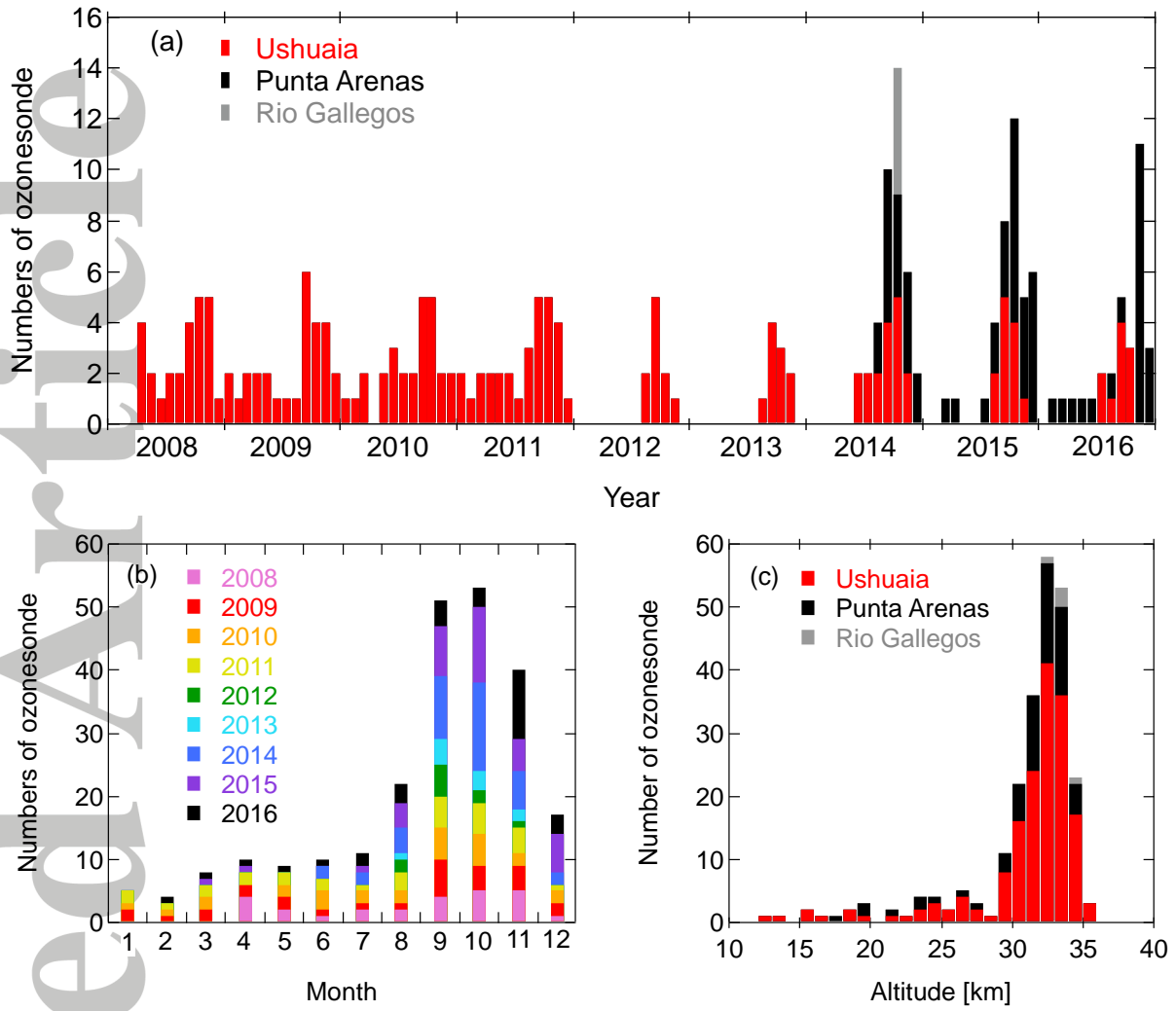
Figure 1. (a) Number of ozonesondes per month at each station. (b) Monthly sounding numbers for each year. (c) Histogram of the maximum heights for each sounding.
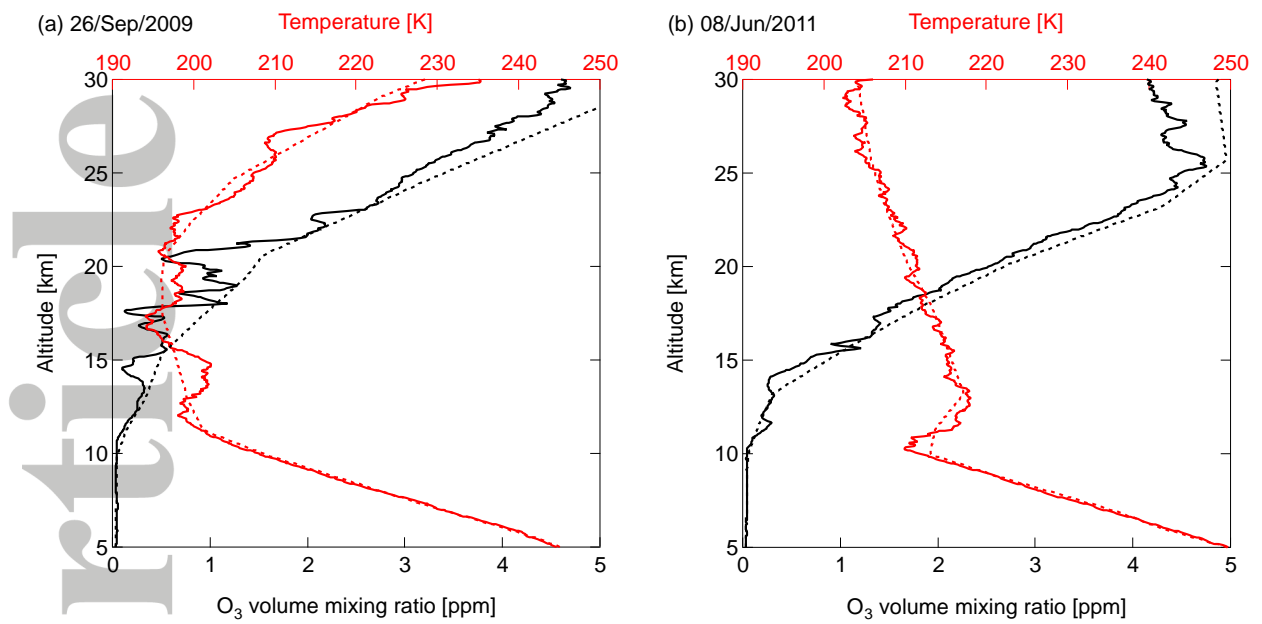
Figure 2. Ozone mixing ratios and temperature profiles recorded by ozonesonde measurements (solid lines) made from Ushuaia station on (a) 26 September 2009 and (b) 8 June 2011. The MERRA-2 ozone mixing ratio and temperature data interpolated temporally and spatially along the flight paths of the sondes are indicated by dashed lines.
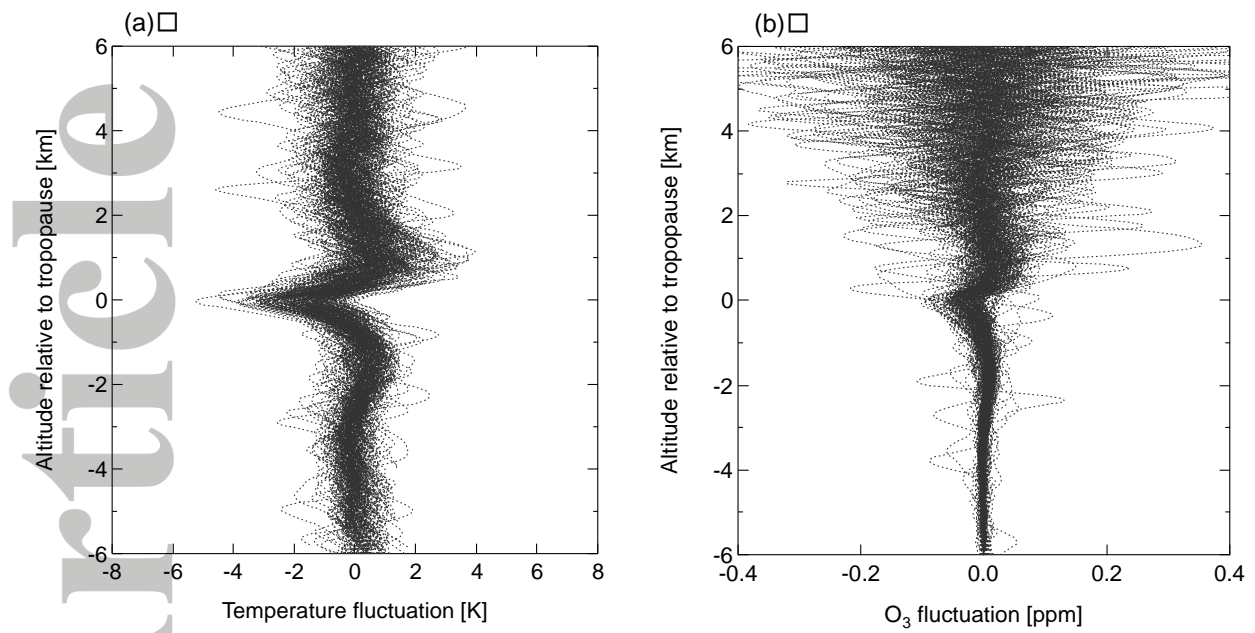
Figure 3. (a) Temperature and (b) ozone mixing ratio fluctuation profiles obtained by applying a high-pass filter with a cutoff of 4 km to the sonde data. The vertical axes correspond to altitude relative to tropopause.
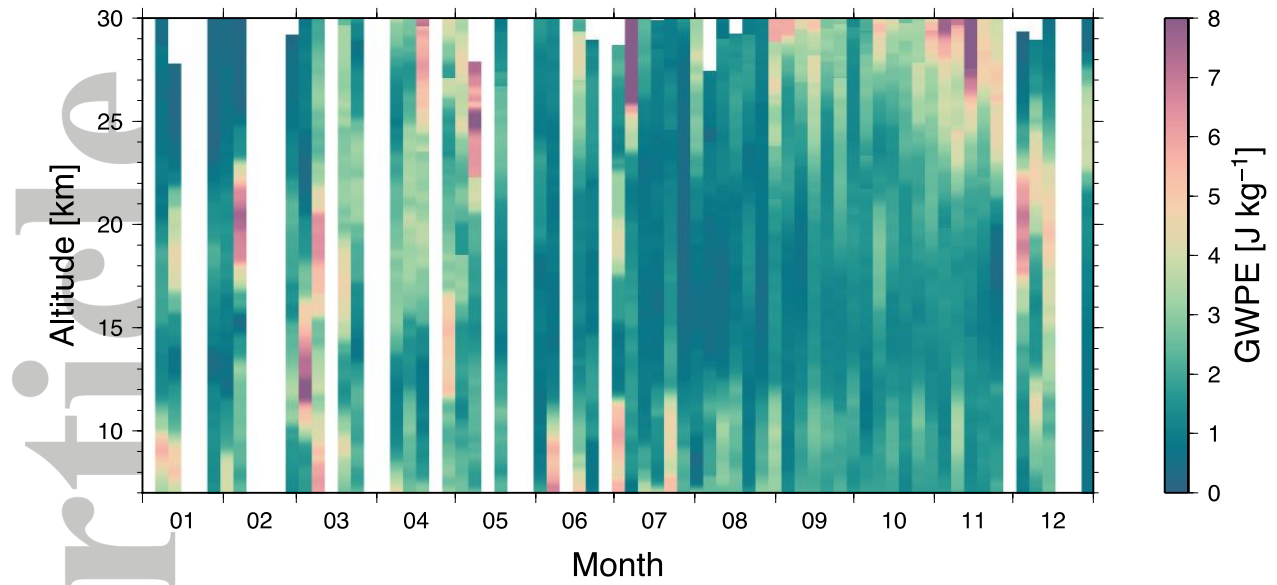
Figure 4. Seasonal variations of the gravity wave potential energy (GWPE), based on sounding data for the whole study period. These variations were obtained by calculating the arithmetic mean within an altitude range of 5 km and by averaging every five days.
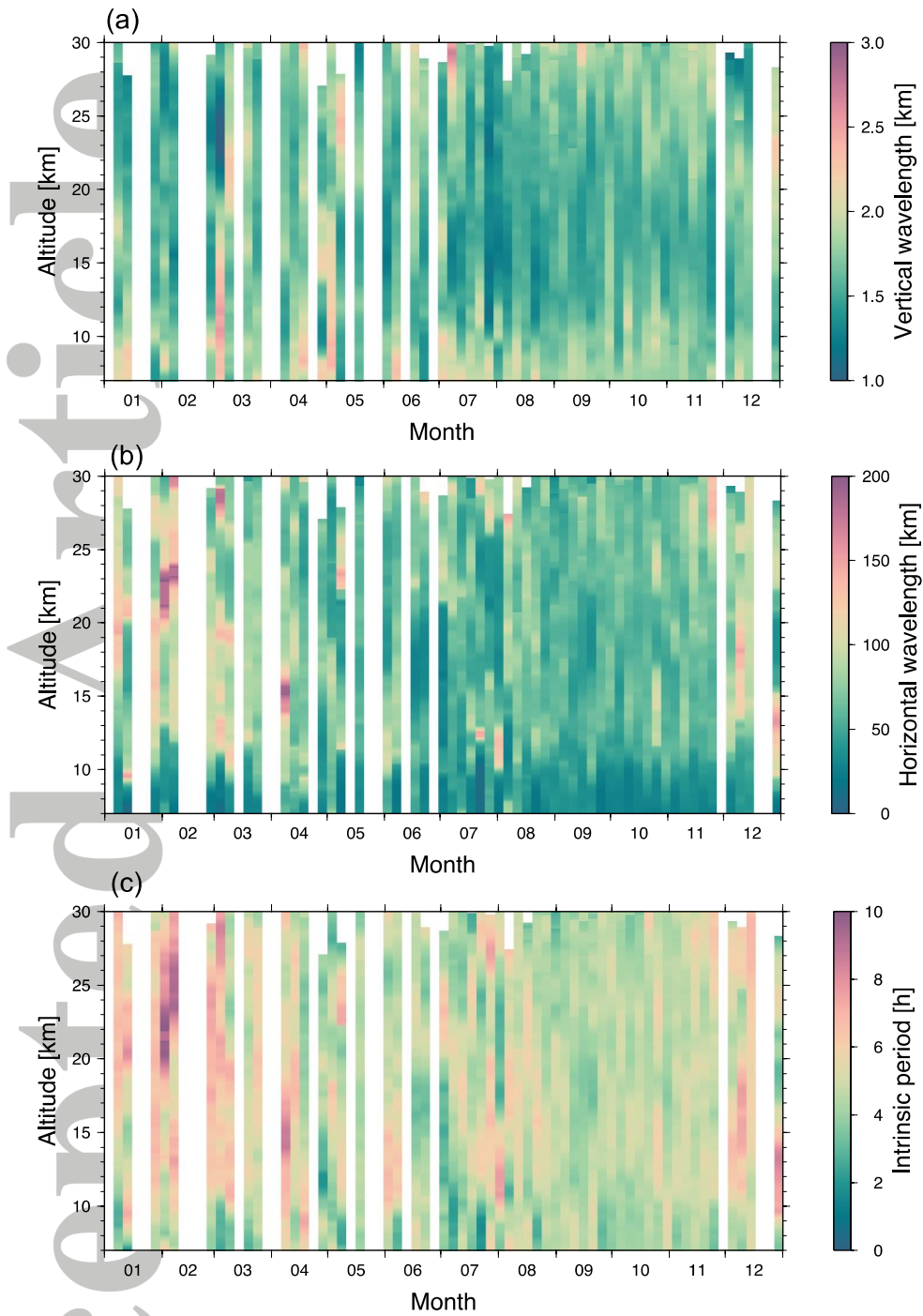
Figure 5. Seasonal variations of (a) vertical wavelength, (b) horizontal wavelength, and (c) intrinsic period of gravity waves. These variations were obtained by calculating the arithmetic mean within an altitude range of 5 km and by averaging every five days using the sounding data for the whole study period.
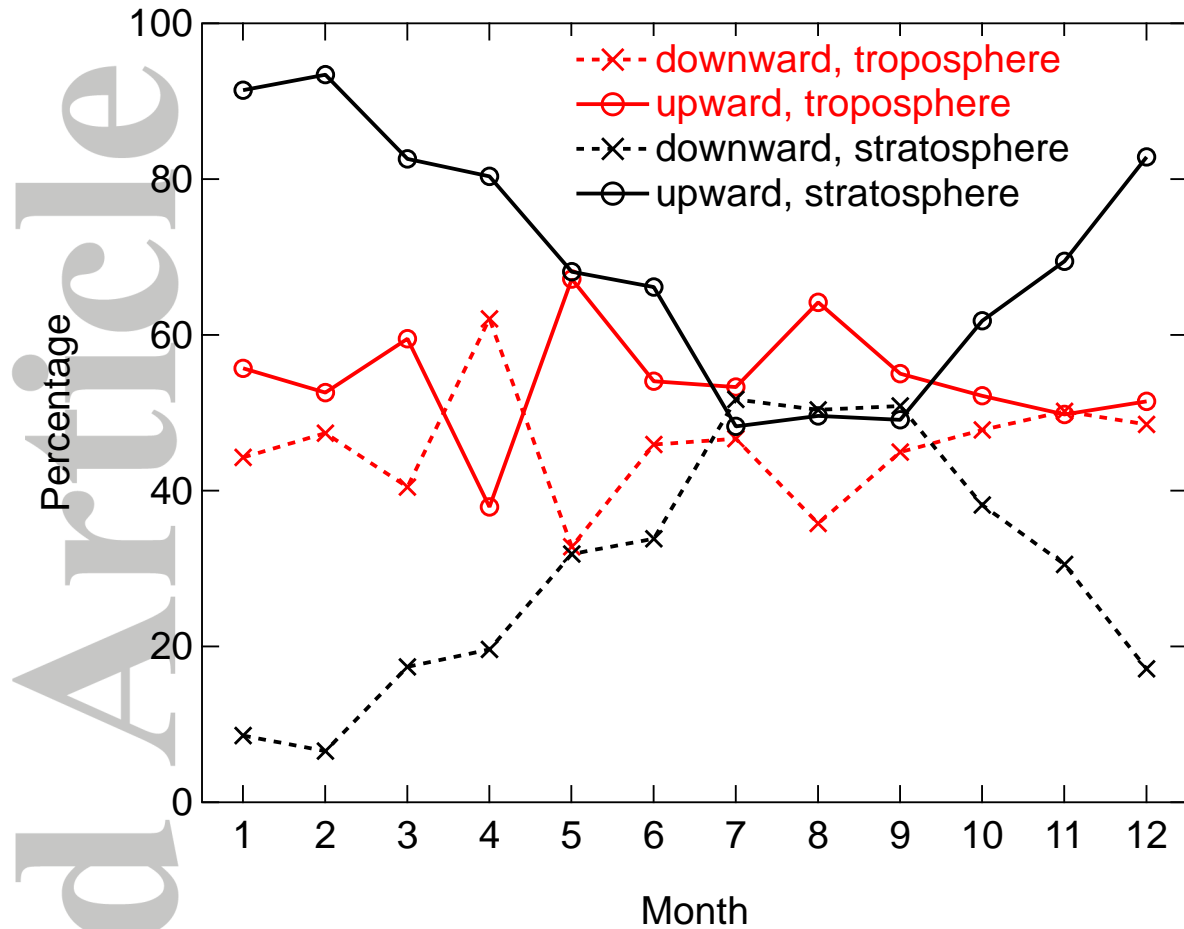
Figure 6. Monthly mean percentages of upward- and downward-propagating gravity waves in the troposphere (red) and the stratosphere (black). The percentages of upward- and downward-propagating waves are denoted by solid and dashed lines, respectively.
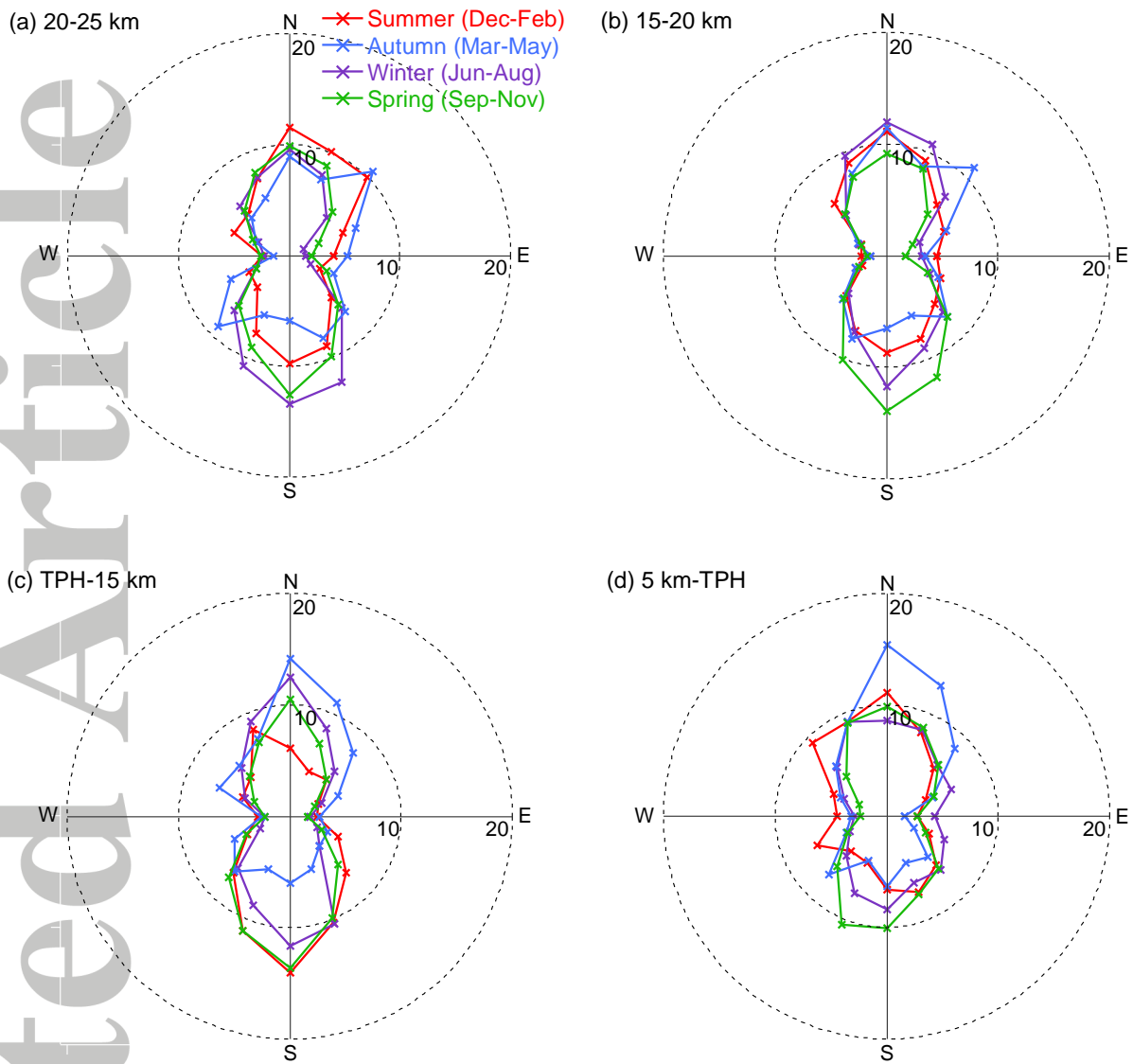
Figure 7. Seasonal probability densities of the horizontal direction of propagation of gravity waves in the altitude ranges of (a) 20–25 km, (b) 15–20 km, (c) tropopause height (TPH)–15 km, and (d) 5 km–TPH.
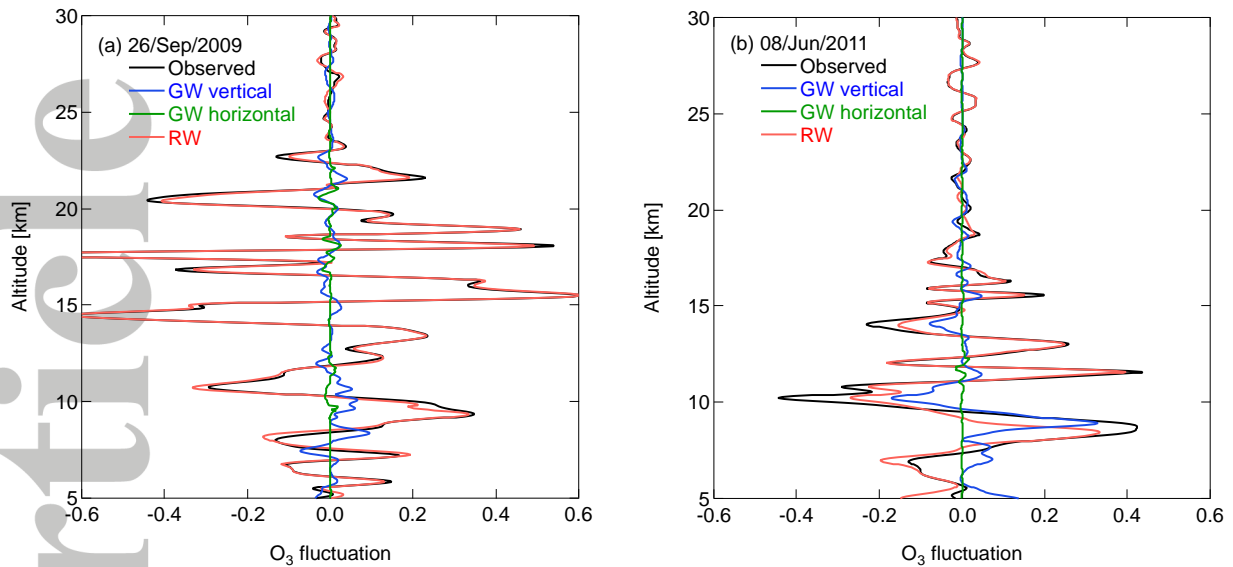
Figure 8. Observed fluctuations of ozone mixing ratios (black), which were equated to the ratio of the perturbation and background components of the ozone concentrations calculated by applying high- and low-pass filters to the observed data, respectively. Fluctuation components of ozone mixing ratios resulting from vertical displacements due to gravity waves (blue), horizontal displacements due to gravity waves (green), and horizontal displacements due to Rossby waves (red) are also shown (see text for details). Figures 8(a) and 8(b) were obtained from the ozonesonde data shown in Figures 2(a) and 2(b), respectively.
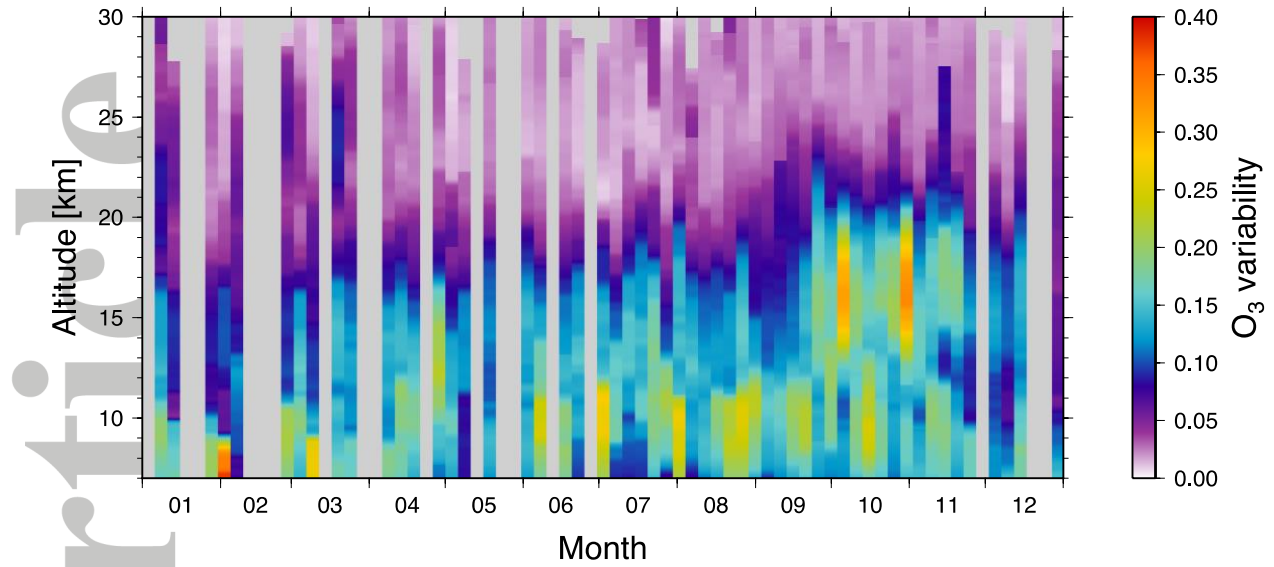
Figure 9. Seasonal variations of the observed ozone variability, based on ozonesonde data for the whole study period. Ozone variability was calculated from the RMS of the observed ozone fluctuations ($\chi'/\overline{\chi}$) within an altitude range of 5 km and averaged every five days.
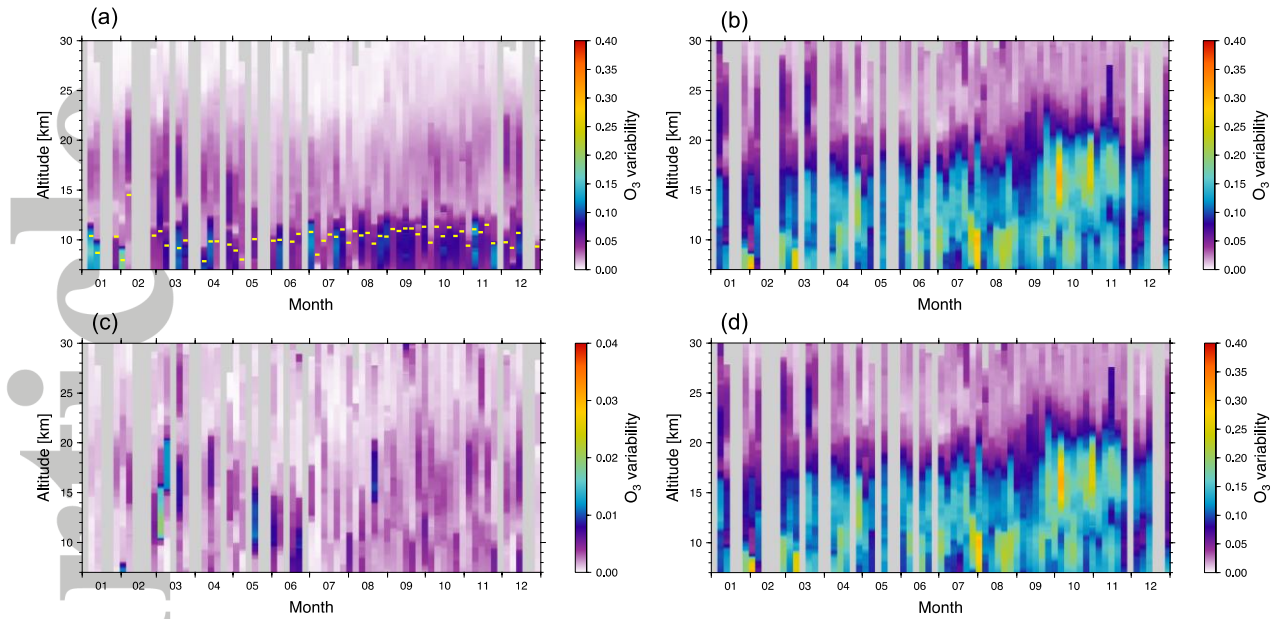
Figure 10. Seasonal variations of ozone variability resulting from (a) vertical displacement, (b) horizontal displacement due to gravity waves and advection due to Rossby waves, (c) horizontal displacement due to gravity waves, and (d) horizontal advection due to Rossby waves. Ozone variability was equated to the RMS of the ozone fluctuations within an altitude range of 5 km and averaged every five days using the ozonesonde data for the whole study period. The yellow bars in Figure 10(a) show the tropopause heights averaged at 5-day intervals.
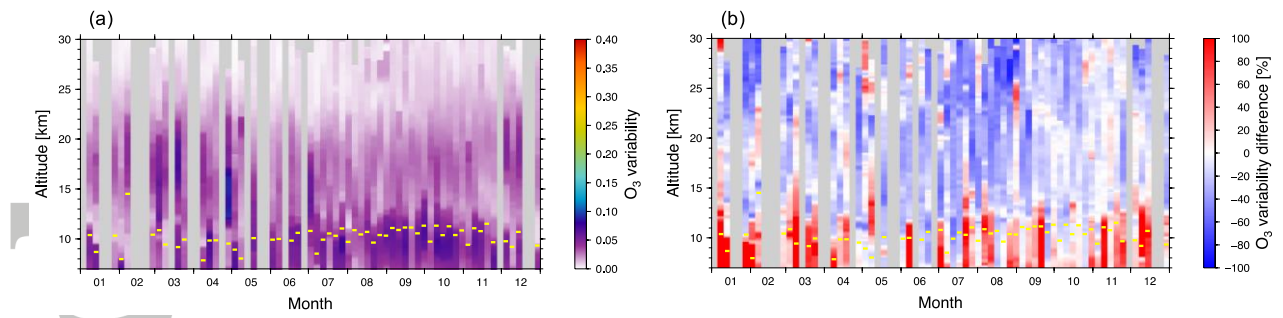
Figure 11. (a) Same as Figure 10(a), but for vertical displacement due to gravity waves calculated from the horizontal wind fluctuations. (b) Relative difference between Figure 10(a) and Figure 11(a) (i.e., (Figure 10(a) − Figure 11(a)) / Figure 11(a) × 100)).
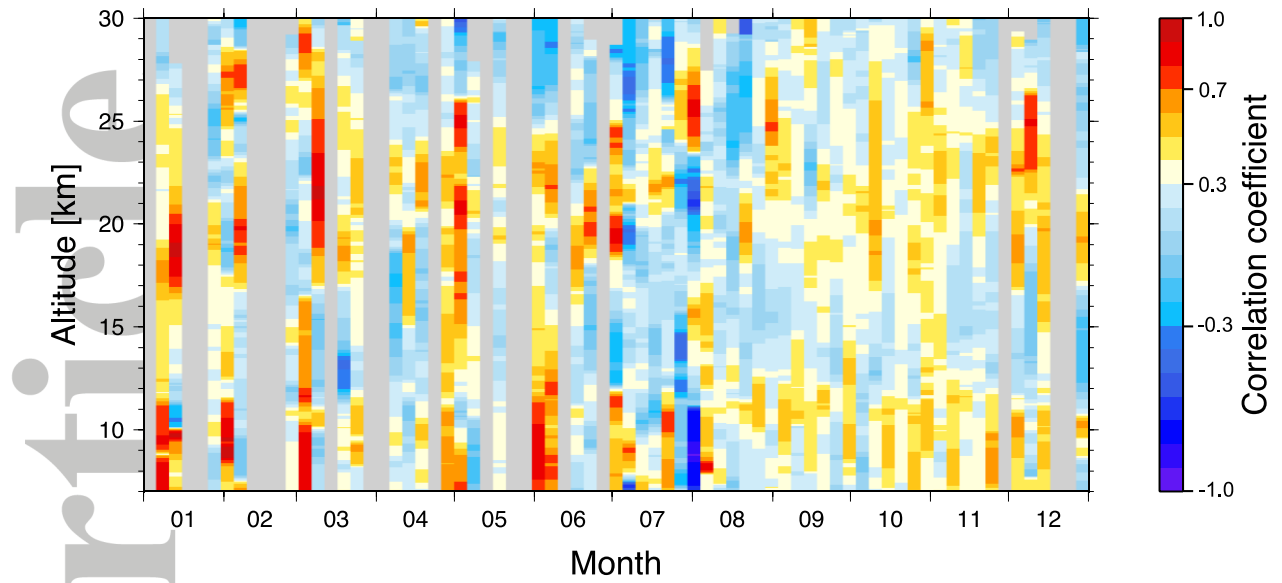
Figure 12. Seasonal variations of the correlation coefficients between ozone and scaled potential temperature fluctuations, which were obtained by averaging every five days using ozonesonde data for the whole study period.
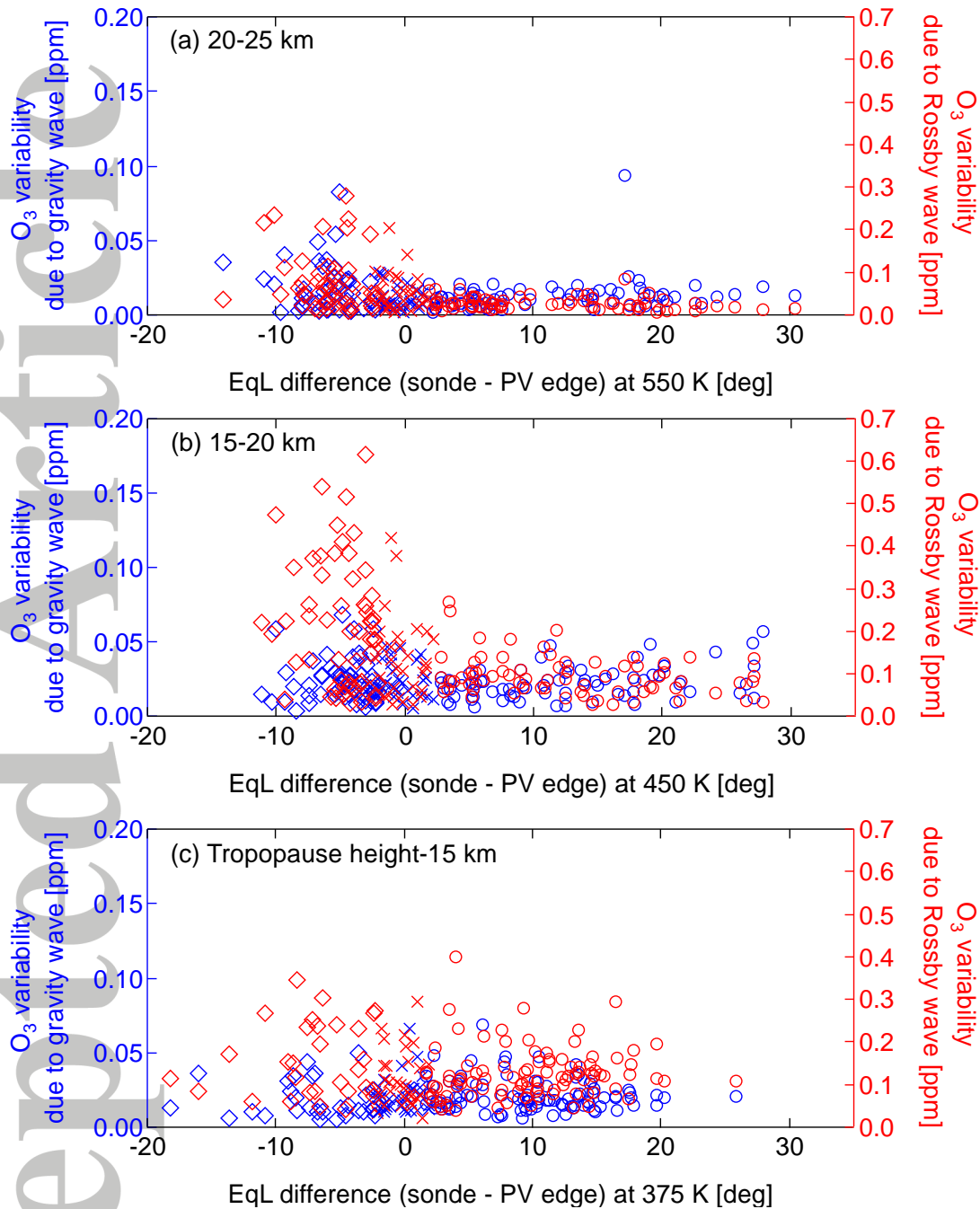
Figure 13. Gravity wave–induced and Rossby wave–induced variability of ozone concentrations between July and November for altitude ranges of (a) 20–25 km, (b) 15–20 km, and (c) tropopause height to 15 km as a function of the differences in the equivalent latitudes (EqLs) between the sonde positions and the polar vortex edges on (a) 550, (b) 450, and (c) 375 K isentropic surfaces. The symbols differ depending on whether the sondes were located inside (diamonds), near the edge (crosses), or outside (circles) the polar vortex (PV). Note that the scales of the gravity wave–induced and Rossby wave–induced variability are different.
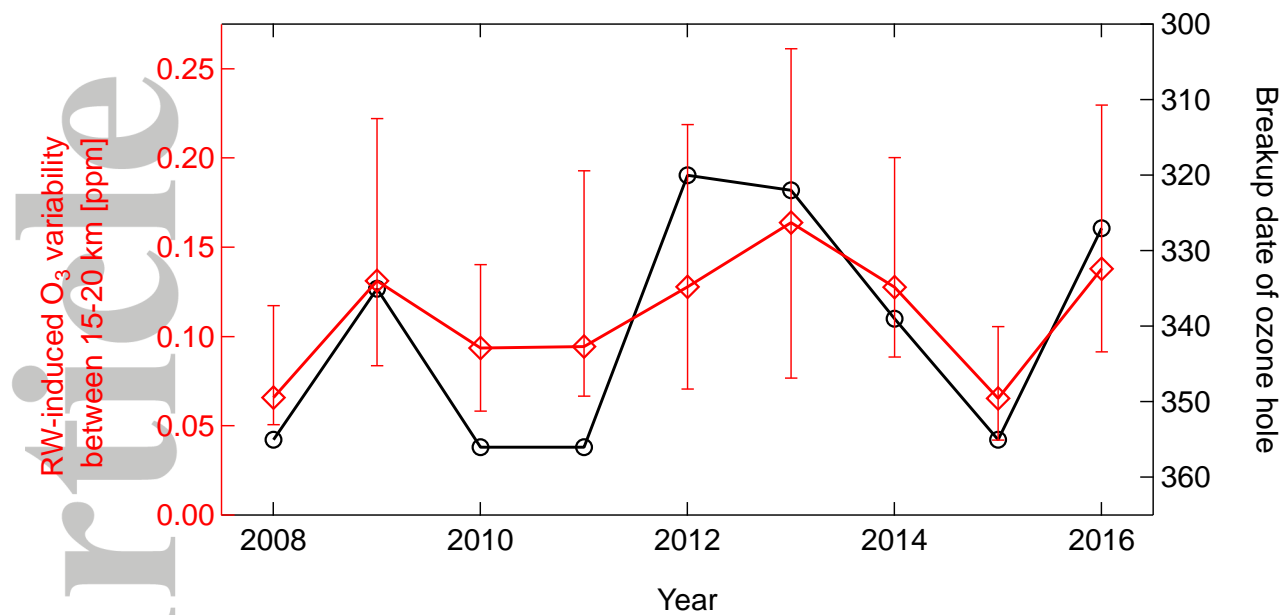
Figure 14. Median of Rossby wave-induced variability between June and November of the year and the day of the final breakdown of the Antarctic polar vortex. The bottom and top edges of the error bars indicate the 25 and 75 percentile limits.